

Upgrade of the Glasgow photon tagging spectrometer for Mainz MAMI-C

J.C. McGeorge,¹ J.D. Kellie,¹ J.R.M. Annand,¹ J. Ahrens,² I. Anthony,¹ A. Clarkson,¹
E.F. McNicoll,¹ P.S. Lumsden,¹ A. Thomas,² R.O. Owens,¹ and G. Rosner¹

¹*Department of Physics and Astronomy, University of Glasgow, Glasgow G12 8QQ, Scotland, UK*

²*Institut für Kernphysik, Universität Mainz, D-55099 Mainz, Germany*

(Dated: August 23, 2021)

The Glasgow photon tagging spectrometer at Mainz has been upgraded so that it can be used with the 1500 MeV electron beam now available from the Mainz microtron MAMI-C. The changes made and the resulting properties of the spectrometer are discussed.

PACS numbers: 29.40.Mc;29.30.Dn

I. INTRODUCTION

The Glasgow photon tagging spectrometer [1, 2] installed at the MAMI-B 883 MeV electron microtron [3, 4, 5] at Mainz, Germany in 1991 has been used in many successful photonuclear experiments. The main focal plane detector [2] consisting of 353 plastic scintillators covered a tagged photon energy range of ~ 40 - 820 MeV at full MAMI-B energy with an energy resolution of ~ 2 MeV and maximum tagged photon flux of $\sim 5 \times 10^5 / \text{MeV} \cdot \text{s}$. Improved resolution over part of the energy range was provided by a 96-element focal plane microscope [6]. Using an aligned diamond radiator tagged photons with linear polarisation greater than 45% have been produced [7, 8, 9, 10, 11] over an adjustable part of the energy range up to ~ 400 MeV. Circularly polarised tagged photons were also generated using polarised electrons from MAMI-B [12]. Several powerful detector systems such as Daphne [13], CATS [14], PIP/TOF [15], TAPS [16] and most recently the Crystal Ball [17] have been used in conjunction with MAMI-B and the Glasgow tagger to make measurements on meson photoproduction and to study photonuclear reactions. Examples include studies of the Gerasimov-Drell-Hearn sum rule [18], the E2/M1 ratio in the $N \rightarrow \Delta$ transition [19] and two nucleon knockout with linearly polarised photons [20].

The recent upgrade of the MAMI accelerator to 1500 MeV, in principle, gives access to interesting tagged photon experiments at higher energy. The photon linear polarisation can also be improved to $>60\%$ up to ~ 800 MeV by using the tighter collimation allowed by the smaller opening angles in the Bremsstrahlung process at higher energy. Examples of such experiments are the detailed study of the second resonance region with complete measurements on pseudoscalar meson production, rare η decay modes to look for physics beyond the standard model and strangeness production near threshold to test chiral perturbation theory. But, as the maximum attainable magnetic field in the original spectrometer was not sufficient to handle an electron energy of 1500 MeV, major modifications were necessary. This paper describes these modifications and the resulting properties of the upgraded spectrometer.

II. AIMS OF THE UPGRADE

The original spectrometer deflected the 833 MeV electron beam through $\sim 79^\circ$ into a beam dump, which was partly recessed into the wall of the experimental hall, and it was decided to try to preserve the original layout as far as possible, so that the tagged photons continue to pass into a large experimental area well shielded from the beam dump. It was also important to preserve the original spectrometer optics which govern the excellent and well understood performance. This in turn avoids the costly redesign of the focal plane detector and its mounting frame. In consequence the magnetic field in the spectrometer had to be increased from 1.0 to ~ 1.8 Tesla in order to deflect the 1500 MeV beam into the original beam dump. In this scheme it was desirable to rebuild the upgraded spectrometer in the same location in the experimental hall.

Although, in principle, the original focal plane scintillators and electronics could still have been used with the upgraded magnet, it was known that the scintillators had become severely radiation damaged. Also, some of the original electronics had become obsolete and incompatible with the CATCH [21] electronics used with the Crystal Ball detector system. Therefore it was decided to replace both the scintillators and the focal plane detector electronics.

III. UPGRADE OF THE SPECTROMETER MAGNET

The existing power supply and cooling arrangements for the magnet coils allowed for a current up to 440 amps which produces a field of 1.4 T [1]. Simple estimates suggested that 1.8 T could be obtained by reducing the pole gap as long as the iron in the return yoke was increased in thickness to prevent saturation. Reducing the pole gap is permissible since angles associated with the Bremsstrahlung process scale approximately as $1/\text{energy}$, and a reduction from 50 mm (for 883 MeV) to 25 mm (for 1500 MeV) does not appreciably increase the fraction of the post-Bremsstrahlung electrons (tagging electrons) which hit the pole faces of the magnet. With a 25 mm

pole gap and 110 mm extra return yoke thickness, calculations using the finite element code TOSCA [22] showed that an average field of ~ 1.96 T would be reached with a current of 440 amps.

The field in the spectrometer is excited by coils positioned around the upper and lower pole shoes in a 'C' magnet configuration as shown in Fig 1. The pole shoes are bolted to the upper and lower yokes which 'sandwich' the 4 back yokes to provide the main magnetic return path. At the input end there is also a short front yoke which has a 'nose' projecting between the upper and lower yokes forming an 'H' magnet configuration. The structure was bolted together with M36 (pole shoes) and M56 bolts (back yokes) which screw into tapped holes. To provide the required extra return yoke thickness additional top, bottom and back yokes were fabricated, each of thickness ~ 110 mm. Appropriate holes were made in the new parts so that (longer) M36 bolts could also pass through them. A 120 mm diameter hole was machined along the photon path through one of the new back yokes.

Measurements [1] had shown that the maximum pole gap distortion in the original spectrometer was 0.14 mm at a field of 1.0 T, and this could be expected to increase to ~ 0.54 mm at 1.96 T. Some estimates of the stresses and distortions involved were made by finite element modelling (FEM) of the original and upgraded spectrometers as solid structures using the IDEAS and ABAQUS programs. This suggested that it would be difficult to apply enough tension to the bolts to stop the new parts slipping on the original parts and therefore difficult to estimate how much extra strength the new parts would provide. Therefore, the design was based on the results from the modelling of the original spectrometer only. The FEM prediction of the pole gap distortion in the original spectrometer was less than that measured by a factor of ~ 1.6 . This is thought to be due to stretching of the M56 bolts which hold the top and bottom yokes to the back yokes. Because there was concern that these bolts might 'pull out' of the tapped holes in the soft iron of the back yokes, it was decided that they would be replaced by through-rods (Fig 1) carrying special nuts which allow a controlled pre-tension to be applied by pneumatic means. The new top and bottom yoke parts were, however, bolted to the new back yokes using M56 bolts into tapped holes.

The FEM showed the importance of the small front yoke in greatly reducing the distortion of the spectrometer at the input end. Aside from the effect on field uniformity, this is important because the vacuum box is made up of the upper and lower poles which 'sandwich' a welded ring of aluminium side walls. This side wall has a 50 by ~ 4000 mm² flanged aperture along the main beam and tagging electron output edges. An outer vacuum box attached to this flange then extends out to the focal plane where a flange carries a thin Kapton window. This structure can distort to follow the pole gap distortion. At the input end, however, there is a vertical, solid aluminium wall whose parts are welded together and it

is important that the distortions in this region are small enough to be taken up by the sealing 'O' rings. The FEM also showed that the stresses in the 'nose' region of the front yoke become rather large at 1.96 T. It was therefore decided to machine this yoke so that the area of the 'nose' could be increased by a factor of about 2. To compensate for the small reduction in the return path cross section brought about by this machining an extra new plate, 113 mm thick, was bolted on to the outside of this yoke.

To reduce the pole gap, 12.5 mm thick shim plates (Fig. 2) were fabricated. The input and all output edges were cut at an angle of 36.1° to continue the chamfer of the existing poles. Counter bored clearance holes allowed these shims to be firmly fixed to the poles by 129 M8 screws. As the pole shims are inside the vacuum, 2 mm diameter holes were drilled through the screws to prevent air being trapped at the ends of the screws and 154, 2 mm diameter holes were drilled through the shims in between the M8 holes to prevent air being trapped between the shims and the pole shoes. In addition, 10, 12 mm diameter holes were made in the lower pole shim to allow alignment pins to be inserted into the existing 3 mm diameter holes in the original lower pole face. These alignment holes define the designed main beam input and output directions and the exit trajectories of 100, 450 and 800 MeV tagging electrons for a main beam energy of 840 MeV.

The magnet support stand was modified so that the upgraded spectrometer could be reinstalled in its original location in the experimental hall and realigned using the original alignment marks set in the floor and height marks set in the walls. Some of the floor marks had been set up along the five electron trajectories defined by the alignment holes in the lower pole shoe.

The new magnet parts were all manufactured from low carbon steel (S275). Although this has a somewhat inferior B/H curve compared to the material (AME2SX1) used in the original spectrometer, it is not very different in the region above 1.5 T. B/H curves were measured (by the Woolfson Centre for Magnetism Technology, Cardiff, UK) for samples of the material used to make the new parts and input to the TOSCA finite-element code to make estimates of the magnetic field. The absence of significant imperfections was checked by ultrasonic testing.

Thin templates were made and compared to the top of the original spectrometer in order to confirm the locations of the bolt holes, so that the new parts could be manufactured while the experimental program at 883 MeV was being completed. These templates were also used to check the new parts at the factory before shipment to Mainz.

After dismantling the original spectrometer the back yokes were machined to make through holes for the strengthening rods and the front yoke was machined to increase the 'nose' area. The stand height was reduced by 110 mm to accommodate the new lower yoke, but this was done in a way which did not change the location of

the 3 support jacks (on which the spectrometer sits) with respect to the stand baseplate.

The vacuum box was modified to provide a larger aperture for the two NMR probes required to cover the extended field range and also to increase the acceptance of the spectrometer to ~ 100 milliradians in the horizontal plane. This is useful for Møller polarimetry which can be used to measure the electron beam polarisation.

Rebuilding of the spectrometer incorporating the new parts took place in 3 stages. In the first stage the new pole shims were aligned to and clamped to the pole shoes so that M8 holes could be drilled and tapped into the latter using the holes in the shims as a template. The M8 screws were then put in place and the clamps were removed.

In the second stage the support stand was reassembled and the new and old lower yokes and the lower pole shoe were put in place and fastened together using new, longer M36 bolts. At this point the main alignment was done using a telescope set up along the input beam line and a theodolite set up along the 450 MeV tagging electron trajectory which is almost orthogonal to the input beam line. The (original) lower pole face was also adjusted to be level and set at the correct height by means of the three support jacks in the support stand.

In the third stage the reassembly was completed. This included pre-stressing the strengthening rods to a tension of about 70 tonnes. As this might have caused some movement of the spectrometer the alignment was then rechecked.

Once the power supply was reconnected to the coils, the pole gap was measured as the current in the tagger coils was increased. The gap reduction was found to have a roughly linearly dependence on the square of the magnetic field indicating that the stresses due to the increased magnetic forces remain in the elastic region. The maximum reduction at full current was found to be ~ 0.42 mm. This is slightly less than predicted from scaling up the distortion measured in the original spectrometer and suggests that the strengthening rods had a beneficial effect.

The photon collimator was re-aligned on the input beam direction using the adjustments built into the V-shaped collimator mounting block. (Several sets of cylindrical lead and heavymet collimators, all with the same outer diameter, are available providing collimating diameters in the range 1 to 8 mm.)

The focal plane detector support structure is fixed to the magnet, but it was surveyed to check that it was remounted in the same position as before to an accuracy of about 1 mm.

IV. MAGNETIC FIELD MEASUREMENTS

Although no detailed field map was made, a temperature compensated Hall probe which had been calibrated against an NMR system was used to make some measure-

ments of the magnetic field produced by the upgraded spectrometer. The field measured at mid-pole gap along line B in Fig. 2 is shown in Fig. 3. It can be seen that the measured field at 435 amps comfortably exceeds the 1.8 T required to handle 1500 MeV. It is also in good agreement with the TOSCA prediction except for the 'dips' at positions 22.5 and 42.5 cm corresponding to the locations of two of the M8 screws which secure the pole shims. Similar results were found along lines A and C. It is not clear whether the 'dips' are predominantly due to saturation of the screw material or to the missing metal which arises from the clearance at the end of the tapped holes and from the holes drilled through the screws to avoid trapped air. Measurements over a few screws indicate that the field reduction has a peak value of $\sim 3.0\%$ and a full width at half maximum of about 17.5 mm. The effect on the energy resolution is thought to be very small due to the small opening angle of the tagging electrons, but there can be some effect on the energy calibration. An estimate of the size of the deviations from a smooth calibration has been obtained by assuming the field is uniform between the poles (except for the 'dips') and zero elsewhere and calculating the total effect on exit position and bend angle caused by all dips whose centre is within 30 mm of the tagging electron trajectory. It is assumed that the fractional effect on bend angle is simply the fractional deficit in the field integral compared to that for a uniform field with no dips. The number of M8 screws involved varies from 1 to 4 or 5 along trajectories at high tagged photon energies, but can be as many as 12 for low photon energies.

Fig. 4 shows the size of the calculated deviation from a smooth calibration as a function of the tagging electron energy, E , expressed as a fraction of the main beam energy, E_0 . As expected, the effect is greatest at low photon energy but is in all cases considerably less than the width of a main focal plane detector channel (~ 13 mm along the focal plane). Although the deviations for the real field may be different in detail, these results indicate that the effects are negligible for most experiments, except perhaps those that make use of the focal plane microscope detector [6] where the channel width is ~ 2 mm along the focal plane. In such experiments a detailed energy calibration can be performed by using one or two different electron beam energies from MAMI and 'scanning' them across the microscope by making small variations in the magnetic field in the spectrometer (see ref [6]). Using 270 MeV electrons from MAMI, this has been done with the microscope at a focal plane position which covers the range $E/E_0 = 0.27 - 0.35$ (for a main beam energy of 883 MeV). The results are shown in Fig. 5, and the deviations from a smooth calibration (a quadratic function is used because the dispersion is not constant, see Fig. 2b of ref [1]) are compared to the predictions in Fig. 6. The agreement is already reasonably good and may be improved by a more detailed scan which would allow an accurate determination of the tagging electron energies corresponding to microscope channel edges. (In the

data shown the extracted hit position (microscope channel centroid) of the electrons has an error because the beam spot width is smaller than the microscope channel width and because, in the analysis, the channel widths were assumed to be equal whereas the width ratio for alternate channels is ~ 2 - see ref [6].)

Both the measurements and the TOSCA calculations indicate (Fig. 3) that in the upgraded spectrometer the field edge is displaced inward from the physical pole edge (see Fig.4 in ref [1]). This was quantified by determining the effective field boundary (EFB) position for five locations based on the field calculated using TOSCA. This was found by making the field integrals, $\int B \cdot dl$, equal for the uniform and calculated fields along lines perpendicular to the pole edge, where the magnitude of the uniform field is taken to be the average field calculated using TOSCA for the region 100-200 mm inside the physical pole edges. The EFB shifts were found to be 21 ± 1 mm at the main beam input and output and at tagging electron exits defined by lines A, B and C in Fig. 2. As the field clamps were not re-optimised for the reduced pole-gap, it is not surprising that the EFB shifts are now larger than in the original spectrometer.

V. FOCAL PLANE DETECTOR

A. The detectors

The focal plane (FP) of the tagger dipole magnet is instrumented with 353 overlapping plastic scintillators which cover an energy range of around 6 - 95% of E_0 , the energy of the primary electron beam. The scintillators are mounted in milled slots to define their positions and angles with respect to the tagging electrons, which are momentum analysed by the dipole magnet. The scintillators have a length of 80 mm, a thickness of 2 mm and widths (9 to 32 mm) which decrease along the focal plane in order to keep the the tagged energy bite roughly constant when the scintillator angles are set so that the tagging electrons are at normal incidence. The scintillator strips overlap by slightly more than half their width so that an electron hit is defined by coincident signals in adjacent detectors and the width of the overlap region (a 'channel') is equivalent to an energy bite of ~ 4 MeV for an incident electron beam energy of 1500 MeV. Neighbouring channels overlap by about 0.4 MeV.

The scintillator EJ200 was chosen for the refurbishment because the scintillation spectrum better matches the response of the phototube and it is thought to be less susceptible to radiation damage than the slightly faster NE 111/Pilot U used in the original setup. The 353 new scintillator detectors were cut from 2 mm thick sheets, and new light guides made from ultra-violet transmitting acrylic were fixed to the scintillator using Dymax 3094 glue cured under an ultra-violet lamp for 14 seconds. They were then wrapped in double sided aluminised Mylar to eliminate optical cross talk and mounted in the

original detector frame [2].

Before installation about half of the scintillators were tested using a Sr90 source and the signal amplitude was found to decrease linearly with increasing width. The signals were larger than those from the old scintillators (on the same PMT) by a factor ranging from ~ 8 to more than 90. This variation is due to the higher radiation damage for those detectors installed at positions corresponding to low tagged photon energy where the tagging electron flux is greatest. Unexpectedly, the damage for detectors in the highest photon energy positions near the radiator was also somewhat bigger than for those in mid-range, possibly due to radiation produced during setup of the main electron beam.

B. Photomultiplier amplifier-discriminator electronics

Each scintillator on the FP is fitted with a Hamamatsu R1635 photomultiplier tube. As the PMTs are affected by stray fields of more than ~ 0.01 T, 0.2 mm thick mild steel plates were fitted on either side of the PMTs along the whole length of the detector array. Along with the standard cylindrical μ -metal screens fitted to every PMT, this was found to be sufficient to cope with the increased stray field from the upgraded magnet when operated at maximum field.

To reduce overall costs it was decided to reuse as many of the original PMTs on the focal plane detector as possible. The selection was made on the basis of gain, which was measured as a function of the applied HV using a stabilised light emitting diode. The 353 best tubes from a stock of around 450 were fitted, starting with the highest gain at the low-electron energy end of the spectrometer and grading progressively downward in gain along the length of the focal plane.

Every PMT is attached to a newly designed amplifier-discriminator (A/D) card (Fig.7). High voltage (HV) is distributed to the PMT electrodes through a Zener stabilised base chain which may be operated from 900 - 1500 V. The HV system is programmed to deliver no more than 1500 V. Typically a PMT is run at around -1100 V, drawing a current of around 0.3 mA. The anode signal is amplified by a factor 10 and fed to a dual, low-high threshold discriminator which supplies a LVDS-logic signal to drive TDCs and scalers. The differential LVDS signal is transported on ~ 10 m of 0.05"-pitch, twist-and-flat cable to active fanout cards which connect to sampling, multi-hit TDCs and scalers (designated CATCH) which were originally designed [21] for the COMPASS experiment at CERN. This type of TDC, which has a channel width of 0.117 ns, removes the need for delay in the TDC input lines which is usually necessary to accommodate the delay in the trigger system. Thus the logic-pulse rise-time is not degraded significantly at the TDC input and the pulse duration can be set to a relatively short 10 ns.

A NIM-logic compatible discriminator output is provided on each A/D card for diagnostic purposes. The amplifier output also connects to a QDC via a $\times 1.3$ buffer stage. This signal is transported on multi-way coaxial delay lines (~ 500 ns) which connect to FASTBUS LeCroy 1885F QDCs. Normally the QDCs are read only during HV adjustment to align the detector gains. The $\times 10$ amplified anode signal, produced by illumination of the R1635 PMT photocathode by a 1 ns duration diode laser, is displayed in Fig. 8. The amplifier produces no discernible degradation of edge speed and the 10-90% rise time was 1.9 ns.

The terminating-resistor network of the CATCH LVDS receiver circuit is hard soldered, so that driving several inputs in “daisy-chain” fashion by a single signal is not feasible. Thus a fanout (Fig. 7) is necessary to drive TDCs, scalers and also auxiliary electronics which, for example, select Møller-scattering events for electron-beam polarisation analysis. This fanout is implemented in low-voltage positive ECL circuitry, 64 channels to a 9U card, with 6 cards (384 channels) located in a purpose built powered crate. Signal ordering on the LVDS input and output connectors is CATCH compatible, which is not compatible with standard 68-way twist and flat cable. A small printed circuit card, connected between the 10 m cables from the tagger and the input to the fanout, converts from standard to CATCH ordering.

Each A/D card draws ~ 370 mA from the +5 V and ~ 250 mA from the -5 V LV supply lines. Type N5700 Agilent switch-mode power supplies [23] provide low voltage for the A/D cards, connecting via 200 A cable to brass bus bars, which run the length of the focal-plane detector. Wiring harnesses attached to the bus bars distribute power to the cards.

High voltage for the PMTs is provided by a CAEN 1527 mainframe [24], populated by 8, type-A1932A, 48-channel distributor cards [25]. The A1932A cards produce a primary HV which is then distributed to all 48 outputs via individually programable step-down circuits. With the primary set to 1500 V the outputs can be programmed within the range 600 - 1400 V. Custom built 48-way cables complete with copper-braid screening and outer insulator connect the distributors to patch panels on the FP detector frame, which feed to the PMTs of the individual FP elements.

C. Detector performance

The performance of the FP detectors and electronics is illustrated in Fig. 9 which displays some spectra taken with the MAMI-C 1500 MeV electron beam incident on a 10 μm Cu radiator. Bremsstrahlung photons, detected by a lead-glass Cherenkov detector placed directly in the beam, triggered the data acquisition system and provided gates for the charge integrating QDCs and the time reference for the TDCs. The top plot shows the pulse height spectrum produced by the tagging electrons in a single

FP detector. This shows very little background below the Landau distribution indicating that the electrons are transported and detected very cleanly in the spectrometer. The middle plot of Fig. 9 shows the difference in hit times for two adjacent FP channels when an electron passes through the small region where the channels overlap. The time variation of the lead-glass trigger cancels in this difference so that the observed width of the distribution for elements i and $i + 1$ is $\delta t \simeq \sqrt{\delta t_i^2 + \delta t_{i+1}^2}$, where δt_i is the timing uncertainty for element i . Assuming $\delta t_i \simeq \delta t_{i+1}$, the Gaussian-fit width (σ) of 0.24 ns is equivalent to a single-counter resolution of 0.17 ns (0.40 ns FWHM). The bottom plot displays the time differences for channels 220 - 352 of the focal-plane detector on a logarithmic z scale, showing that this level of time resolution is typical in that region. This is significantly better than the pre-upgrade system where the best performance obtained was ~ 1 ns FWHM.

VI. TESTS

A first estimate of the intrinsic resolution of the upgraded spectrometer was made at a field of 1.95 T which made an 855 MeV beam from MAMI hit the microscope placed near the middle of the focal plane. A 2 mm Al ‘scatterer’ was introduced in the beam near the radiator position to simulate the opening angle distribution of tagging electrons. The resolution was found to be ~ 0.4 MeV FWHM. This is an overestimate because the opening angles in this test were about 3 times bigger than is the case for the tagging electrons from a typical radiator at 1500 MeV main beam energy. It shows that when the main focal plane detector is used its channel width (~ 4 MeV) dominates the tagged energy resolution. For some experiments which make use of the focal plane microscope, however, it may be necessary to make more careful measurements of the resolution.

Measurements of the ‘tagging efficiency’, that is the fraction of the tagged photons which pass through the collimator, were made at reduced beam current using a 25 cm^3 lead-glass Cherenkov detector placed on the photon beam line. The results of measurements with 6 micron Ta and 10 micron Cu radiators and 3 and 4 mm diameter collimators were found to be 10 - 20 % smaller than predicted by Monte Carlo calculations which include the effects of input beam divergence and diameter, the Bremsstrahlung photon opening angle distribution and multiple scattering, but not the effects of Møller scattering. As in the original setup [2], this discrepancy may be due to a slight misalignment of or imperfections in the collimator.

As a test of the focal plane detector background, the count rate was measured with no radiator in the beam. It was found to be about 5×10^{-5} times smaller than the rate with a 10 μm thick Cu radiator in the beam.

The maximum useful tagged-photon intensity depends on the maximum rate at which the FP counters can be

run. Up to a rate of ~ 1 MHz per channel (detector singles rate of ~ 2 MHz) no major change of pulse height was observed, so that the detection efficiency for minimum ionising particles did not change significantly.

VII. TAGGER ENERGY CALIBRATION

In the analysis of an experiment with the tagger it is necessary to know the energies of the tagging electrons which hit the centres of each focal plane detector channel. As the MAMI beam energy can be measured with an uncertainty of 140 KeV [26] this calibration has been carried out directly using very low current MAMI beams of lower energy than in the main experiment, although it is only practical to obtain a small number of calibration points in this way. On the assumption that the field shape along any electron trajectory is independent of field magnitude, an attempt was made to 'simulate' intermediate tagging electron energies, $E' = EB/B'$ by varying the tagger field (B') away from the field B for which the spectrometer is being calibrated using MAMI energy E . The error that arises because the field shape is not independent of field magnitude can be quantified by making several overlapping calibrations using different beam energies.

Even if this method were sufficiently accurate, it is still not practical to calibrate directly all 352 focal plane detector channels, and some interpolation is necessary. To guide this interpolation a computer program has been written to calculate the calibration on the basis of a uniform tagger field (see Sect. IV). The relative positions and angles of the scintillators are known from the construction of the support frame [2] and the position and angle of the frame location relative to the magnet was determined by surveying. For electron trajectories made up of circular arcs and straight lines the required calibration can be calculated by simple geometry.

The strength of the field is taken from the value measured using a Drusche NMR system multiplied by a factor, f , which accounts for the difference between the field at the NMR probe (see Fig. 2) and the average field encountered by the tagging electrons. The value of f was adjusted to best fit the measured calibration (see below).

In the measurement the MAMI beam is 'scanned' across the focal plane detectors by varying the tagger field. By making fine steps it is possible to measure the field values for which the beam hits the small overlap regions (see Sect. V A) between neighbouring channels. This gives the hit position to an accuracy of about 0.1 channel.

Calibration measurements have been made with MAMI energies 195.2, 405.3, 570.3, 705.3 and 855.2 MeV and the resulting calibration for a field of 1.834 T (which is used when tagging with 1508 MeV main beam energy) is compared to that calculated assuming a uniform field in the upper part of Fig. 10. The difference between the measured and calculated calibration is shown in the lower part.

From the overlapping points from the 195.2/405.3 and 705.3/855.2 MeV scans it can be seen that the effects of field shape changes are small (~ 0.5 MeV) around tagger channel 100, but increase for higher channels. However, at five points (shown by the crosses in Fig. 10) corresponding to the five MAMI energies used in the calibration, the error from this effect can be virtually eliminated by interpolation of the observed hit position as a function of the magnetic field. The choice of f was based on these five points.

For 1508 MeV the calculated calibration underestimates the tagged electron energy by about 1 MeV (~ 0.25 channels) for low channels and overestimates it by about 1 MeV around channel 215. When MAMI energies between 900 and 1400 MeV become available the measurements will be extended to higher channels.

Similar results have also been obtained for a field of 1.057 T, which is used when tagging with a main beam energy of 883 MeV. The value of f was found to vary between 1.0013 for 1508 MeV and 1.0098 for 883 MeV. Further measurements, over a wider field range, will allow accurate parameterisation of this factor in the calculation.

Using this method it is not possible to measure the energy calibration for tagging electron energies much below 180 MeV which is the lowest energy routinely available from MAMI. Extrapolation into this region can be made using the uniform field model described above, but it is difficult to estimate the uncertainty. The possibility of measuring the calibration in this region using Møller electron pairs where one of the pair is in the low energy region of interest and the energy of the other is measured using the microscope detector positioned in the corresponding high electron energy region, is being examined but may not be feasible if the wide angle (~ 80 milliradians) trajectory of the low energy member of the pair changes the calibration.

VIII. SUMMARY

The upgrade of the Glasgow photon tagging spectrometer at Mainz has been completed successfully. When used with the 1508 MeV beam from MAMI-C, it provides tagged photons in the energy range 73-1402 MeV with a photon flux up to $\sim 2.5 \times 10^5$ photons per MeV and energy resolution of ~ 4 MeV. Energy calibration has been made using the accurately known MAMI energies.

The upgraded spectrometer has been in regular use for tagged-photon experiments with the Crystal Ball and TAPS since the beginning of 2007, using incident energies of 883 MeV and 1508 MeV. Experiments to investigate η and K meson photoproduction on the proton have already yielded very promising preliminary results and will continue with various polarised and unpolarised targets.

A. Acknowledgements

We would like to thank R. Thomson, Department of Mechanical Engineering, University of Glasgow for assistance in setting up the stress analysis, S. Kruglov and the technicians at the Petersburg Nuclear Physics Institute, St. Petersburg, for cutting the new scintillators, V. Bekrenev (St. Petersburg) V. Lisin and S. Cherepnya (Moscow) for testing the PMTs and J. McGavigan (Glasgow University), R. Hoffman and K.S. Virdee (George Washington University) for laboratory assistance in test-

ing the amplifier/discriminator cards. We also thank D. Doak, Science Faculty workshop, Glasgow University and the workshop staff in Mainz for technical assistance, and C-H. Kaiser, A. Jankowiak and the Mainz accelerator group for providing electron beam of excellent quality at several energies.

This research was supported by the UK EPSRC, the Deutsche Forschungsgemeinschaft (SFB 443) and DAAD (ARC-program ARC-X-96/21) and is part of the EU integrated infrastructure initiative hadron physics project under contract number RII3-CT-2004-506078.

-
- [1] I. Anthony, J.D. Kellie, S.J. Hall and G.J. Miller, Nucl. Instr. and Meth. **A301** (1991) 230.
 - [2] S.J. Hall, G.J. Miller, R. Beck and P. Jennewein, Nucl. Instr. and Meth. **A368** (1996) 698.
 - [3] H. Herminghaus, K.H. Kaiser and H. Euteneuer, Nucl. Instr. and Meth. **A138** (1976) 1.
 - [4] T. Walcher, Prog. Part. Nucl. Phys. **24** (1990) 189
 - [5] J. Ahrens et al., Nuclear Physics News **4** (1994) 5.
 - [6] A. Reiter et al., Eur. Phys. J. **A30** (2006) 461.
 - [7] D. Lohman et al., Nucl. Instr. and Meth. **A343** (1994) 494.
 - [8] U. Timm, Fortschritte der Physik **17** (1969) 765.
 - [9] F. Rambo et al., Phys. Rev. **C58** (1998) 489.
 - [10] F.A. Natter, P. Grabmayr, T. Hehl, R.O. Owens and S. Wunderlich, Nucl. Instr. and Meth **B211** (2003) 465.
 - [11] K. Livingston, 'The Stonehenge Technique: a New Method of Crystal Alignment for Coherent Bremsstrahlung Experiments', International Conference on Charged and Neutral Particle Channeling Phenomena, Frascati (2005) 170.
 - [12] K. Aulenbacher, Nucl. Instr. and Meth. **A391** (1997) 498.
 - [13] G. Audit et al., Nucl. Instr. and Meth. **A301** (1991) 473.
 - [14] F. Wissmann et al., Phys. Lett. **B335** (1994) 119.
 - [15] I.J.D. MacGregor et al., Nucl. Instr. and Meth. **A382** (1996) 479, P. Grabmayr et al., Nucl. Instr. and Meth. **A402** (1998) 85.
 - [16] R. Novotny, IEEE Trans. Nucl. Science, **38** (1991) 379.
 - [17] M. Oreglia et al., Phys. Rev. **D25** (1982) 2259, S. Starostin et al., Phys. Rev. **C64** (2001) 055205.
 - [18] J. Ahrens et al., Phys. Rev. Lett. **87** (2001) 02203.
 - [19] R. Beck et al., Phys. Rev. Lett. **78** (1997) 606.
 - [20] C.J.Y. Powrie et al., Phys. Rev. **C64** (2001) 034602, S. Franczuk et al., Phys. Lett. **B450** (1999) 332.
 - [21] A common readout driver for the COMPASS experiment, T. Schmidt, Ph.D. thesis, Albert-Ludwigs-Universität, Freiburg, May 2002.
 - [22] A.G.A.M Armstrong, C.P. Riley and J. Simkin, TOSCA: 3D Static Electromagnetic/Electrostatic Analysis Package, RL-81-070 (Rutherford Appleton Laboratory, 1982), TOSCA: 3D Magnetic Field Computation (Vector Fields Ltd., 24 Bankside, Kidlington, Oxford, UK.)
 - [23] Agilent Technologies 2004, <http://www.agilent.com>, pdf file 5969-2917.pdf.
 - [24] Universal Multichannel Power Supply, CAEN 2005, <http://www.caen.it/nuclear>, pdf file sy1527usermanual_rev13.pdf.
 - [25] 48 Channel 3kV Distributor Board, CAEN 2006, pdf file A1932A_REV7.pdf.
 - [26] K.-H. Kaiser, private communication, A. Jankowiak et al., Eur. Phys. J. A direct (2006) DOI: 10.1140/epja/i2006-09-016-3.

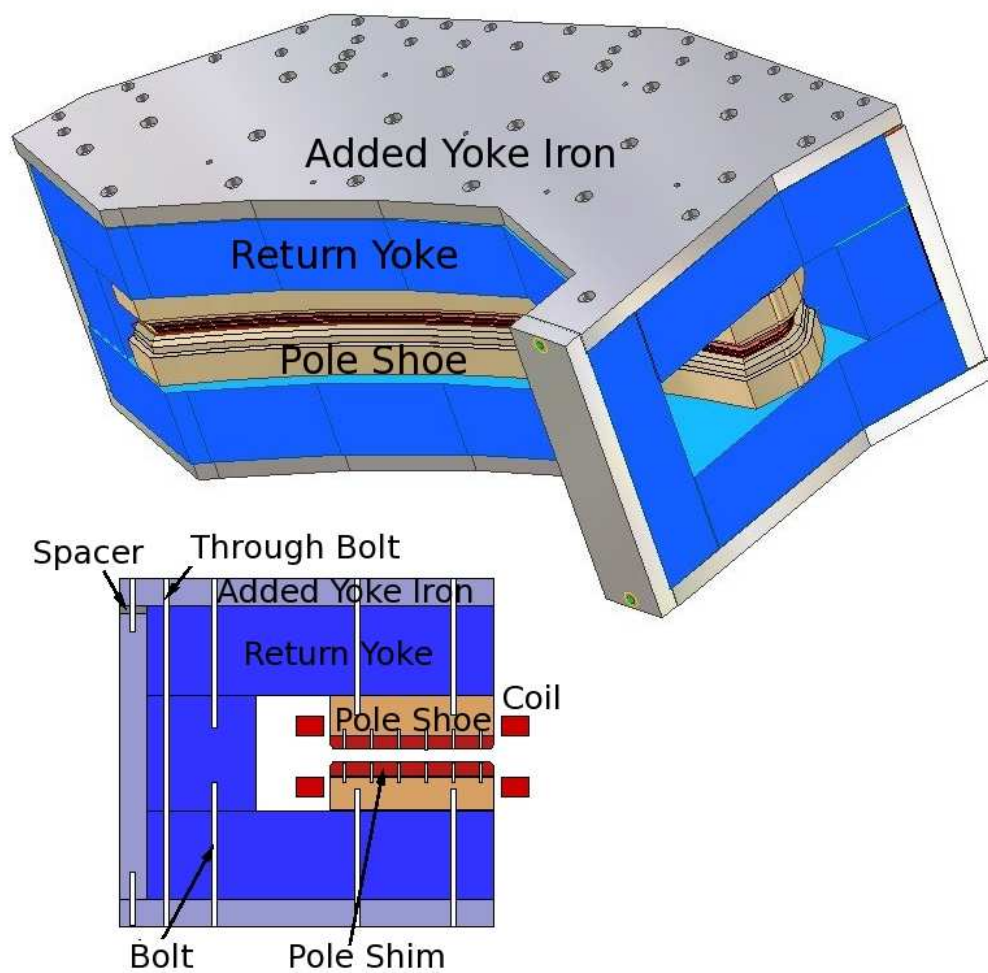


FIG. 1: The upgraded photon tagging spectrometer - 3D view (upper) and cross section (lower).

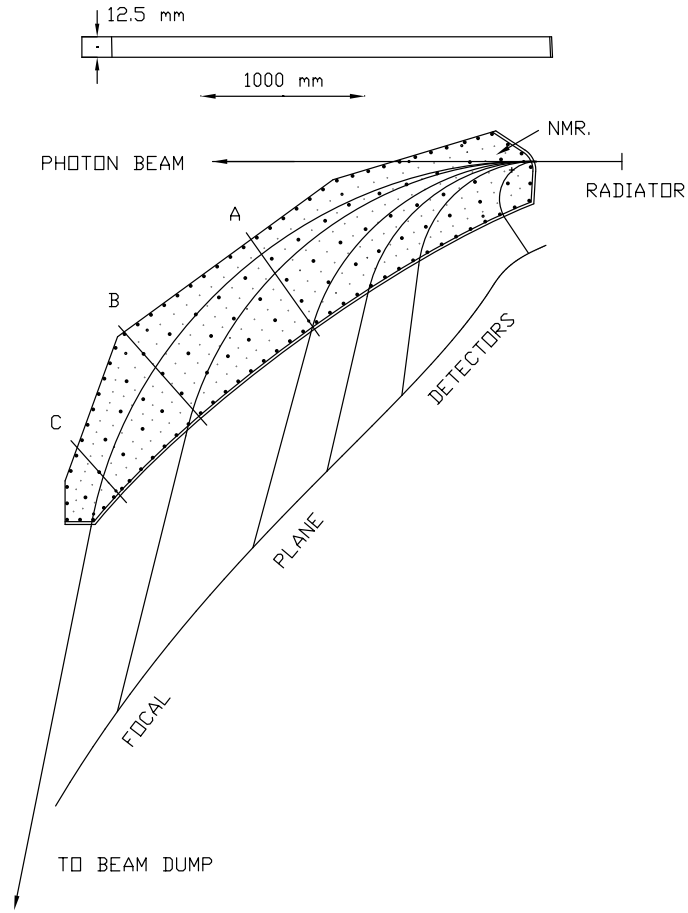


FIG. 2: The lower pole shim. (The upper pole shim is similar.) The small circles indicate the locations of the M8 screws and the dots show the 2 mm vacuum relief holes. The vertical scale in the elevation drawing is exaggerated by a factor of 10. The photon beam, main electron beam, four tagging electron trajectories and the location of the main focal plane detectors are superposed on the plan drawing.

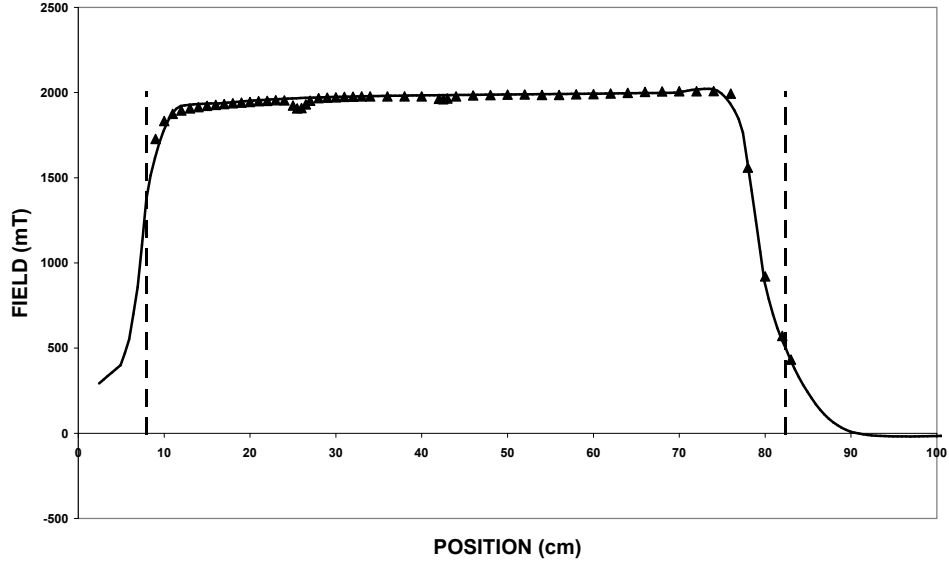


FIG. 3: The magnetic field at 435 A in the upgraded spectrometer measured along line B in Fig. 2 compared to the TOSCA prediction (line). The dashed lines show the position of the pole edges.

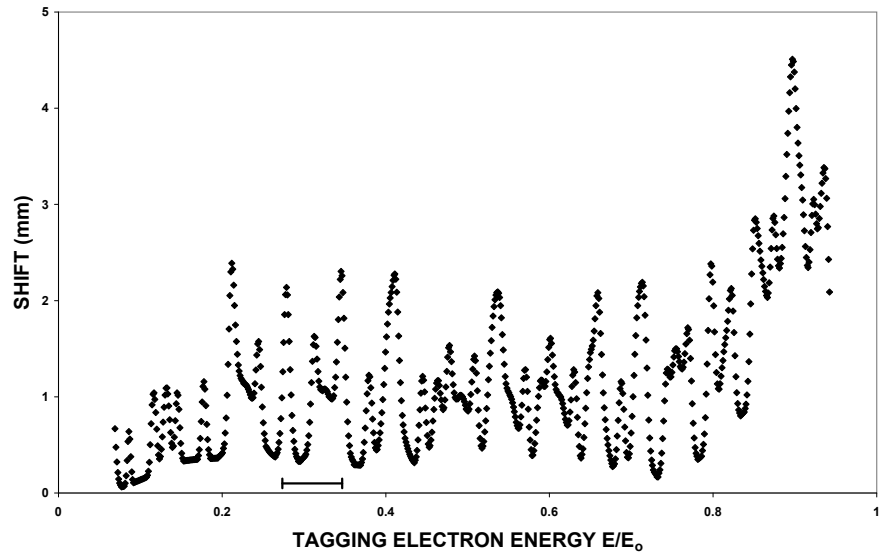


FIG. 4: Calculated shift of the tagging electron trajectories along the focal plane due to the field dips caused by the M8 screws fixing the pole shims. The horizontal bar shows the region covered by the microscope for the energy calibration data shown in Figs. 5 and 6.

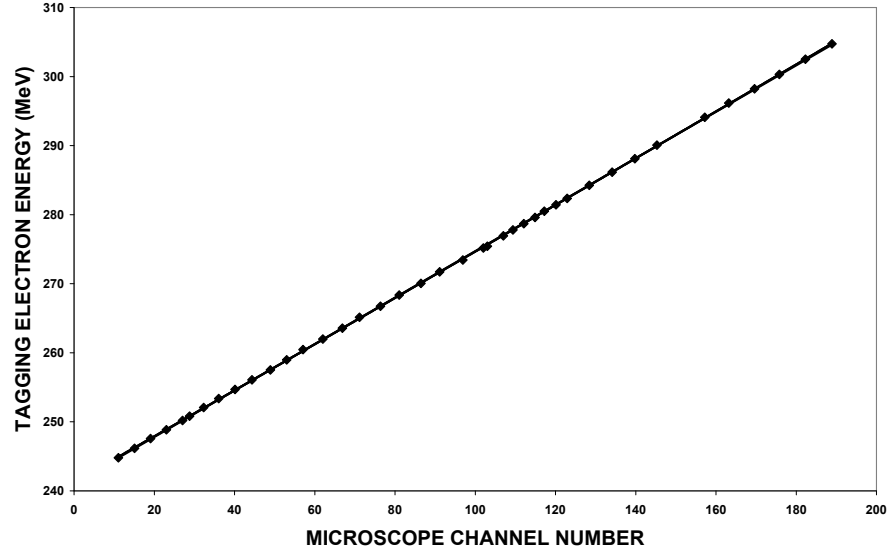


FIG. 5: Tagger energy calibration in the microscope region (for a main beam energy of 883 MeV) obtained from scanning a 270.17 MeV beam from MAMI across the microscope by varying the tagger field. The line shows a quadratic fit.

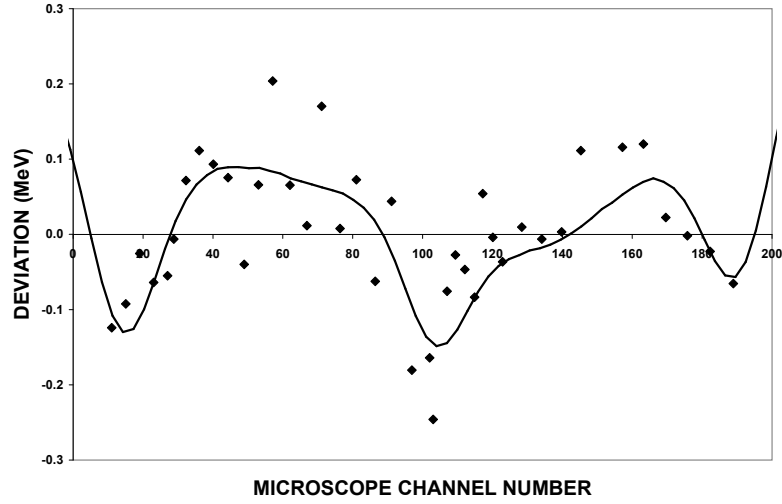


FIG. 6: Deviations from the fit to the energy calibration shown in Fig. 5. The line shows the calculated deviation based on the appropriate section of Fig. 4.

FP Scintillator HV and Discriminator

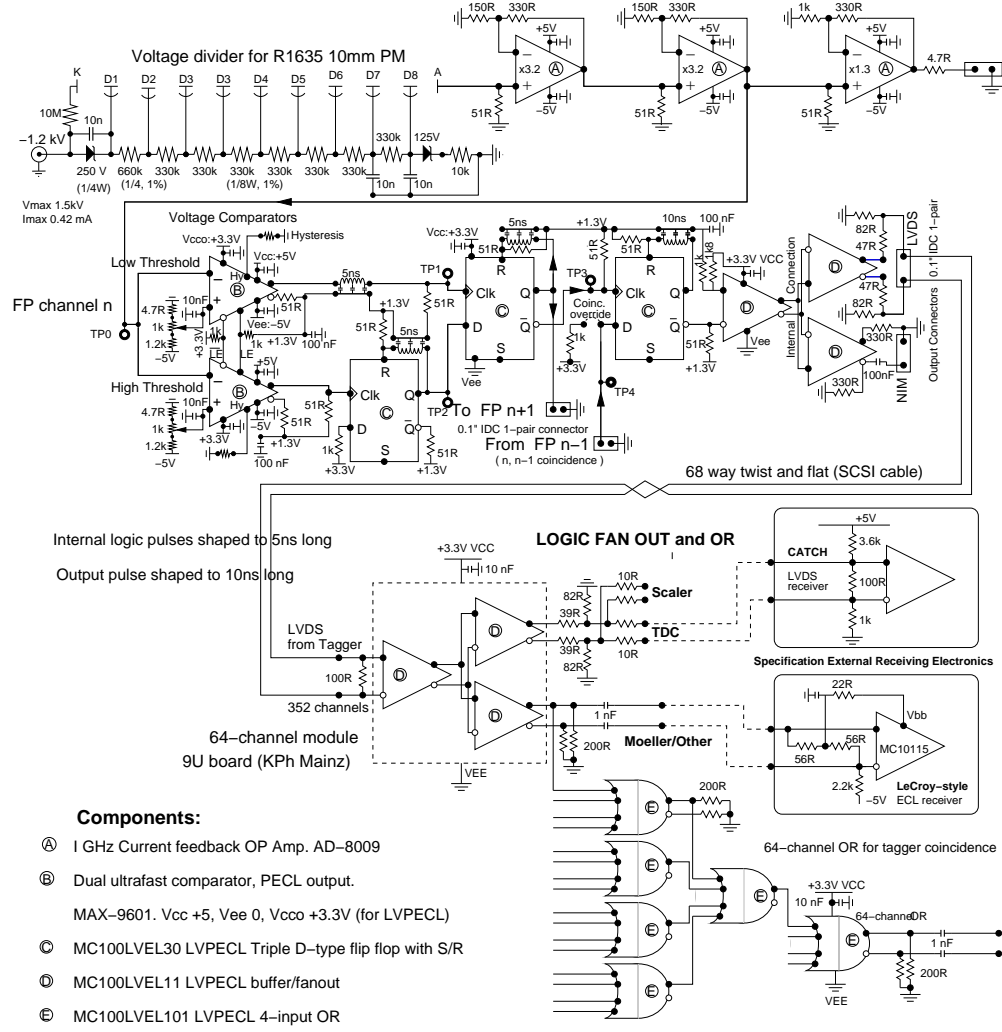


FIG. 7: Circuit diagram of the amplifier-discriminator card and the logic fanout.

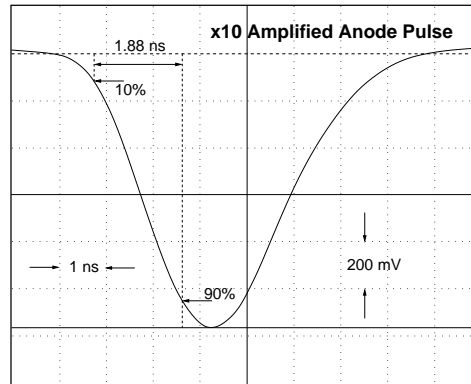


FIG. 8: Amplifier output.

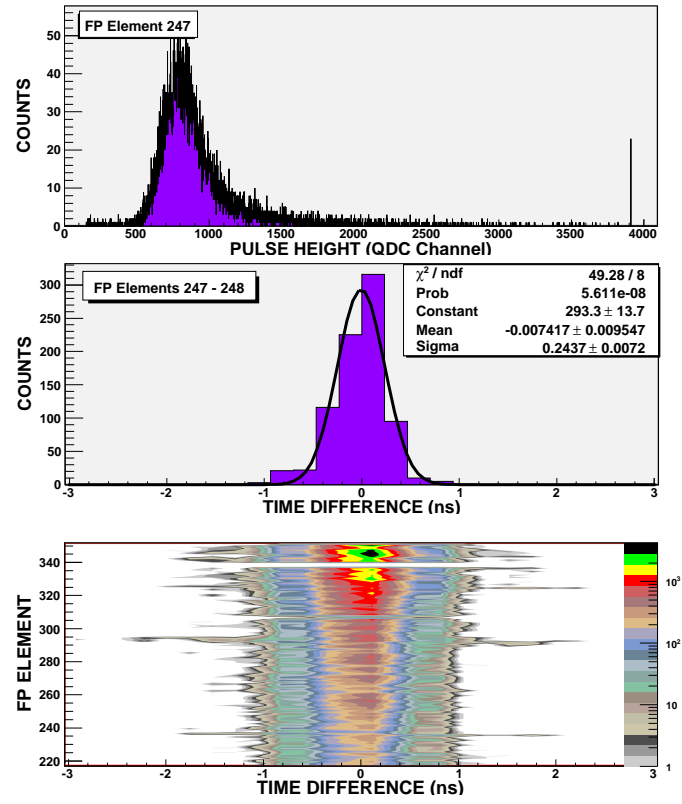


FIG. 9: Focal plane detector performance.

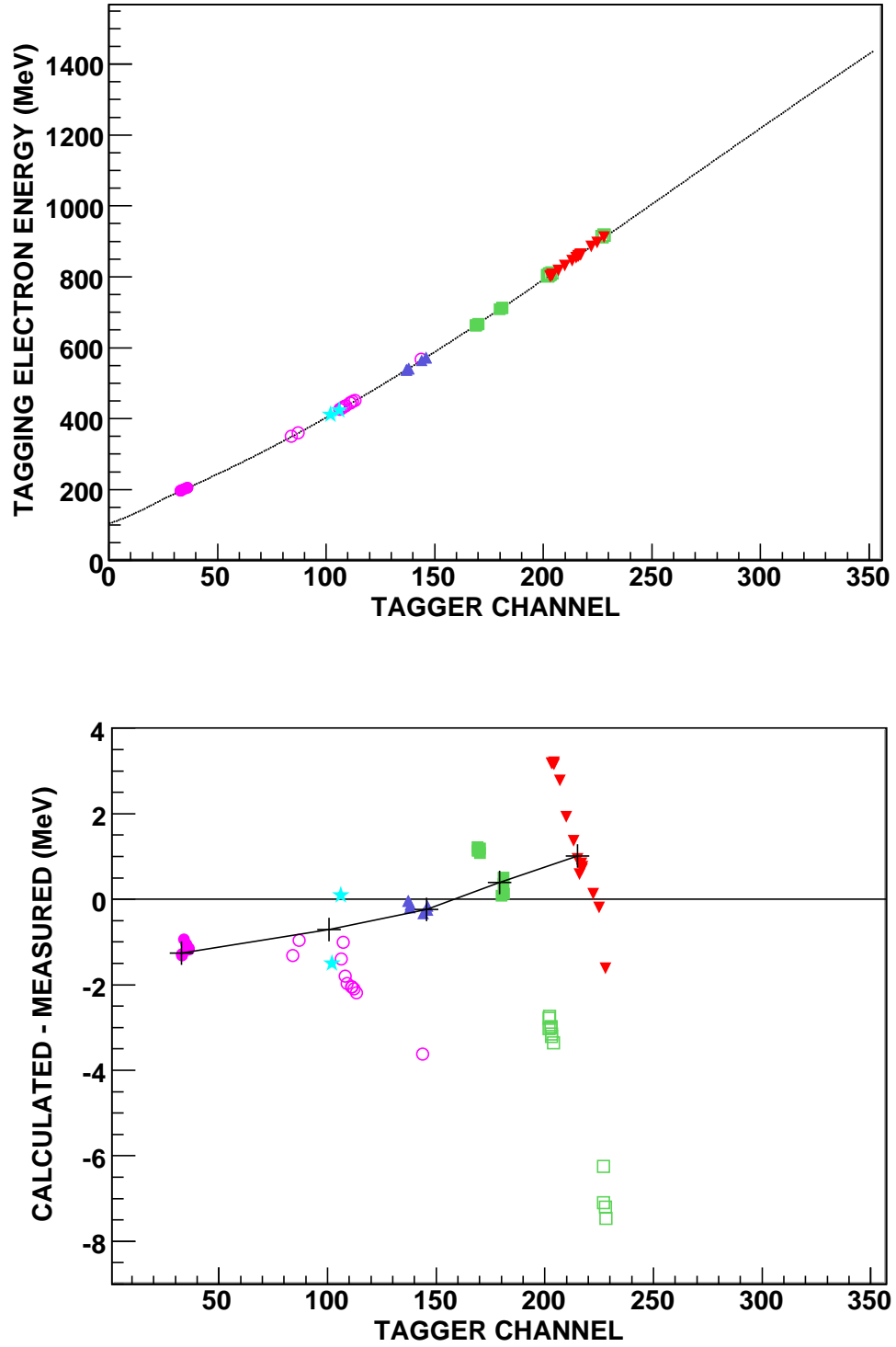


FIG. 10: Upper part: Tagger energy calibration for main beam energy 1508 MeV measured by scans (see text) using MAMI energies 195.2 (circles), 405.3 (stars), 570.3 (triangles), 705.3 (squares) and 855.2 MeV (inverted triangles). The filled in symbols represent points obtained with the tagger field within 10% of the correct value for 1508 MeV. The open symbols show points obtained from a larger field variation. The line shows the calibration calculated assuming a uniform field. Lower part: Difference between the calculated and measured calibrations. The crosses show the five points where the field in the scans is equal to that which correctly dumps 1508 MeV in normal tagging. The line joining the crosses is to guide the eye.

